CHAPTER 6: RESULTS

The barrier height distribution in identically prepared metal Schottky contacts on n-Ge (100)

6.1 Introduction

The Schottky barrier height (SBH) is one of the most interesting properties of a MS interface [1]. The electronic properties of the MS contacts are characterized by their SBH. The SBH is, therefore, of vital importance to the successful operation of any semiconductor device [1]. The mechanisms that determine the SBH are still not fully understood [2,3,4,5]. It is only in the past two decades that an inhomogeneous contact has been considered as an explanation for a voltage-dependent SBH [1,2,6]. The SBH is likely to be a function of the interface atomic structure and the atomic inhomogeneities at MS interface, which are caused by grain boundaries, multiple phases, facets, defects, a mixture of different phases, etc. [7,8,9,10]. It has also been suggested by Song et al. [11] that the barrier inhomogeneities can occur as a result of inhomogeneities in the interfacial oxide layer composition, nonuniformity of the interfacial charges and interfacial oxide layer thickness. The presence of barrier inhomogeneities may greatly influence the current across the MS contact [11]. Tung et al. [10,12] assumed lateral variations of SBH to model imperfect Schottky structures, and they depicted larger ideality factors and smaller effective SBHs when they increased the inhomogeneity of barriers. The experimental effective SBHs and ideality factors obtained from the current-voltage (*I-V*) and capacitance-voltage (*C-V*) characteristics differ from diode to diode even if they are identically prepared [10, 12,13,14,15]. This finding has been attributed to interfacial patches, i.e. small regions with lower SBH than the junction's main SBH [1,12].

Although studies have been performed to investigate the relationship between the effective BHs and ideality factors of the metal/Si Schottky diodes [16,17,18,19,20], nothing has yet been reported on the relationship between effective SBHs and ideality factors from forward bias *I-V*

and reverse bias *C-V* characteristics of the metals/Ge Schottky diodes. In this study palladium (Pd), nickel (Ni) and gold (Au) Schottky diodes on n-type germanium were fabricated under experimentally identical conditions in order to investigate the relationship between the effective BHs and ideality factors obtained from the forward bias *I-V* and reverse bias *C-V* characteristics of these metals Schottky diodes. The homogeneous SBH values for Pd/n-Ge (111), Ni/n-Ge (100) and Au/n-Ge (100) Schottky diodes were obtained from the linear relationship between the experimental effective SBHs and ideality factors which is experimentally [15,21,22,23,24] and theoretically [10,12 ,25] confirmed. The homogeneity or uniformity of the SBH is an issue with important implications on the theory of SBH formation [26], and important ramifications for the operation of Schottky diodes [13,15,23 24]. The importance of this homogeneous BH is that, it depicts the real meaningful value characteristic for the MS system [18], which should be used to develop theories of physical mechanisms determining these BHs of Schottky contacts [27]. The rest of the Chapter is organised as follows: Section 6.2, briefly describes the experimental procedure. Results and discussions are presented in Section 6.3. A summary of the work is given in section 6.4.

6.2 Experimental procedures

We used bulk-grown, (100)-oriented, n-type Ge, doped with antimony (Sb) to a density of about 2.5×10^{15} cm^{-3} and supplied by Umicore. Before metallization, the samples were first degreased and subsequently etched in a mixture of H_2O_2(30%):H_2O (1:5) for 1 minute. Immediately after cleaning, the samples were inserted into a vacuum chamber where AuSb (0.6%Sb), 100 nm thick, was deposited by resistive evaporation on the back surfaces as Ohmic contacts. The samples were then annealed at 350°C in Ar atmosphere for 10 minutes to minimise the contact resistivity of the Ohmic contacts [28]. Before Schottky contacts deposition, the samples were again chemically cleaned as described above. Pd, Ni and Au Schottky contacts were deposited onto Ge wafers by using vacuum resistive evaporation at a pressure below 10^{-6} Torr. The contacts were 0.6 mm in diameter and 30 nm thick. The thickness of the metal layer and the deposition rates were monitored with the help of a quartz crystal thickness monitor. After the contact fabrication, the Schottky barrier diodes (SBDs) were characterized by using *I-V* and *C-V* measurements at room temperature.

6.3 Results and discussions

The BHs of the contacts were deduced from the *I-V* characteristics, which were analysed by using the thermionic emission model given by the following equation [2,29]:

$$I(V) = I_0 \exp\left(\frac{qV}{nkT}\right)\left[1 - \exp\left(-\frac{qV}{kT}\right)\right] \tag{6.1}$$

with

$$I_0 = A^* A T^2 \exp\left(-\frac{q\Phi_B}{kT}\right) \tag{6.2}$$

where I_0 is the saturation current derived from straight line intercept of the $\ln(I) - V$ plot at $V = 0$, V is the bias voltage, T is the absolute temperature, q is the electronic charge, k is the Boltzmann constant, A is the effective diode area, A^* is the effective Richard constant, Φ_B is the zero bias effective SBH. From Eq. (6.2) we have:

$$\Phi_B = \frac{kT}{q} \ln\left(\frac{A^* A T^2}{I_0}\right) \tag{6.3}$$

and n is the ideality factor, which is a measure of conformity of the diode to pure thermionic emission. The values of n are calculated from slope of the linear part of an $\ln(I)$ *versus* V plot, assuming pure thermionic emission

$$n = \frac{q}{kT} \frac{dV}{d(\ln I)} \tag{6.4}$$

which is equal to 1 for an ideal diode and usually has a value greater than unit for practical diodes.

We fabricated 20 contacts (Schottky barrier diodes) for Pd-/, Ni-/ and Au/n-Ge (100) on the same n-type semiconductor substrate by evaporation of Pd, Ni or Au as the Schottky contact. Figs. 6.1 - 6.3 show the room temperature experimental forward and reverse bias *I-V*

characteristics of Pd/n-Ge (100), Ni/n-Ge (100) and Au/n-Ge (100) Schottky barrier diodes (SBDs). The *I-V* effective BHs for the Pd, Ni and Au diodes varied from 0.513 to 0.558 eV, 0.487 to 0.508 eV and 0.507 to 0.598 eV, respectively, and ideality factors for Pd, Ni and Au diodes ranged from 1.11 to 1.57, 1.34 to 1.53 and 1.12 to 2.03, respectively.

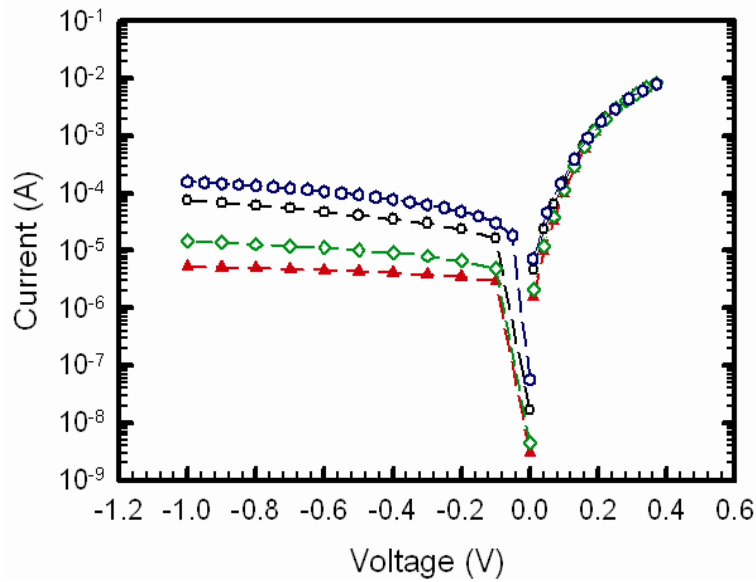

Fig. 6.1 *The plot of the forward and reverse bias current-voltage (I-V) characteristics for five Pd/n-Ge (100) Schottky diodes at room temperature.*

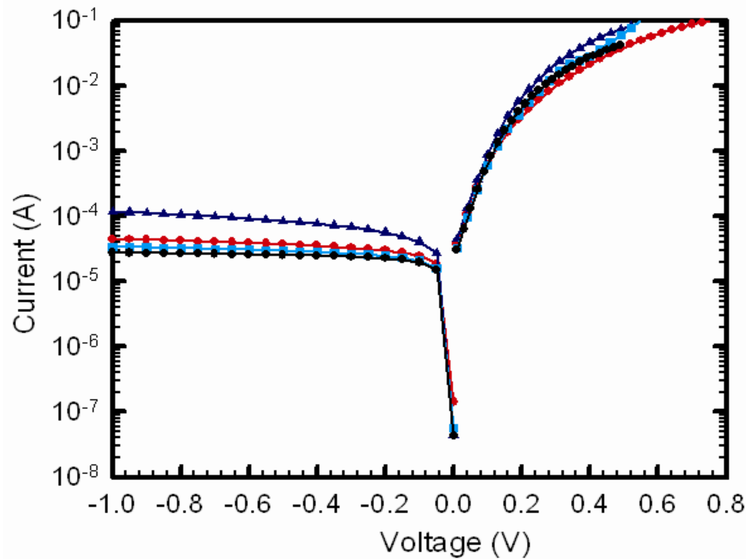

Fig. 6.2 *The plot of the forward and reverse bias current-voltage (I-V) characteristics for four Ni/n-Ge (100) Schottky diodes at room temperature.*

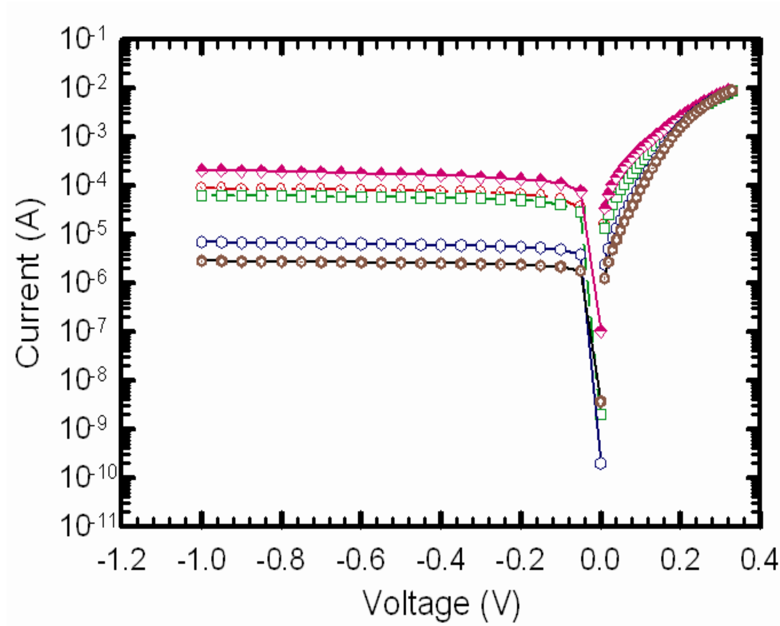

Fig. 6.3 *The plot of the forward and reverse bias current-voltage (I-V) characteristics for five Au/n-Ge (100) Schottky diodes at room temperature.*

Thus, the experimental effective SBHs and ideality factors from the *I-V* characteristics can differ from diode to diode even though they were identically prepared on the same sample.

In Schottky diodes, the depletion layer capacitance, *C* can be expressed as [2]:

$$\frac{1}{C^2} = \frac{2(V_i - V)}{q\varepsilon_s A^2 N_D} \tag{6.5}$$

where A is the area of the diode, ε_s is the dielectric constant of the semiconductor, V_i is obtained from the intercept of C^{-2} with the voltage axis and is given by:

$$V_i = V_d - kT / q \tag{6.6}$$

and N_D is the donor concentration of the n-type semiconductor substrate. From Eq. (6.5), the values of N_D can be determined from the slope of the $C^{-2} - V$ plot. Figs. 6.4 - 6.6 show room temperature reverse bias $C^{-2} - V$ characteristics for selected samples of the Pd/n-Ge (100), Ni/n-

Ge (100) and Au/n-Ge (100) Schottky diodes recorded at 1 MHz. The values of the BH $\Phi_B(C-V)$ can be obtained from Figs 6.4 - 6.6 as

$$\Phi_B(C-V) = V_d + \xi - \Delta\Phi_B \qquad (6.7)$$

where ξ is the energy difference between the bulk Fermi level and the conduction band edge, V_d is the diffusion potential and $\Delta\Phi_B$ is the image force barrier lowering and is given by [2,29]

$$\Delta\Phi_B = \left[\frac{qE_m}{4\pi\varepsilon_s\varepsilon_0}\right]^{\frac{1}{2}}, \qquad (6.8)$$

where ε_0 is the free space dielectric constant and E_m is the maximum electric field and is given by

$$E_m = \left[\frac{2qN_D V_0}{\varepsilon_s\varepsilon_0}\right]^{\frac{1}{2}} \qquad (6.9)$$

The plots of C^{-2} as a function of reverse bias voltage (Figs 6.4-6.6) are linear, which indicate the formation of Schottky diodes [30] and a nearly constant donor concentration profile in the region close to the substrate surface.

The capacitance-voltage BH for Pd/n-Ge (100), Ni/n-Ge (100) and Au/n-Ge (100) diodes ranges from 0.320 to 0.381 eV, 0.358 to 0.418 eV and 0.286 to 0.429 eV, respectively. These results depict that the parameters of Schottky diodes vary from diode to diode even if they are identically prepared. Therefore, their averages should be used [12,13,14,21,25].

Figs. 6.7 - 6.9 show the histograms of BHs from the forward bias *I-V* plots of Pd/n-Ge (100), Ni/n-Ge (100) and Au/n-Ge (100) MS structures, respectively. Figs. 6.10-6.12 show the statistical distribution of BHs from $C^{-2}-V$ plots of the same diodes. Gaussian distribution function was used to obtain fits to the histograms.

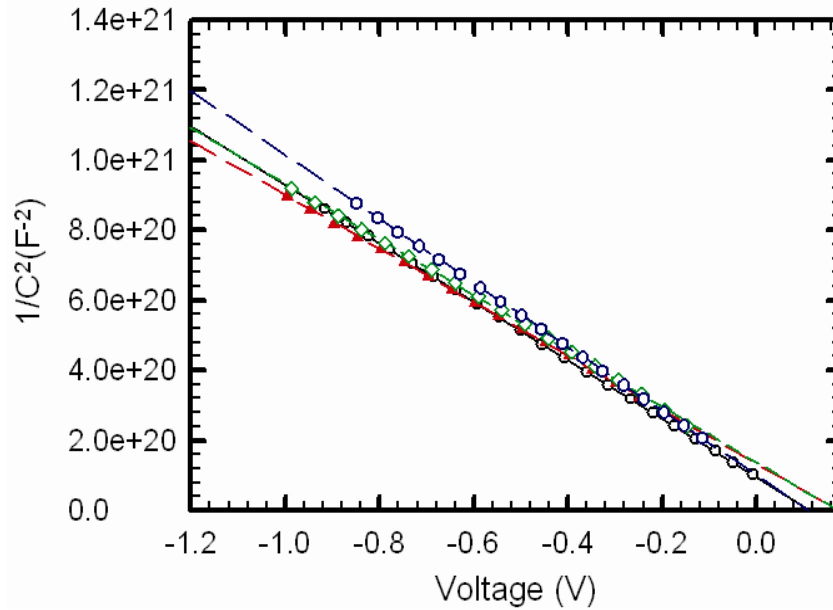

Fig. 6.4 *Reverse bias* $C^{-2}-V$ *characteristics for five Pd/n-Ge (100) Schottky diodes recorded at 1 MHz and room temperature.*

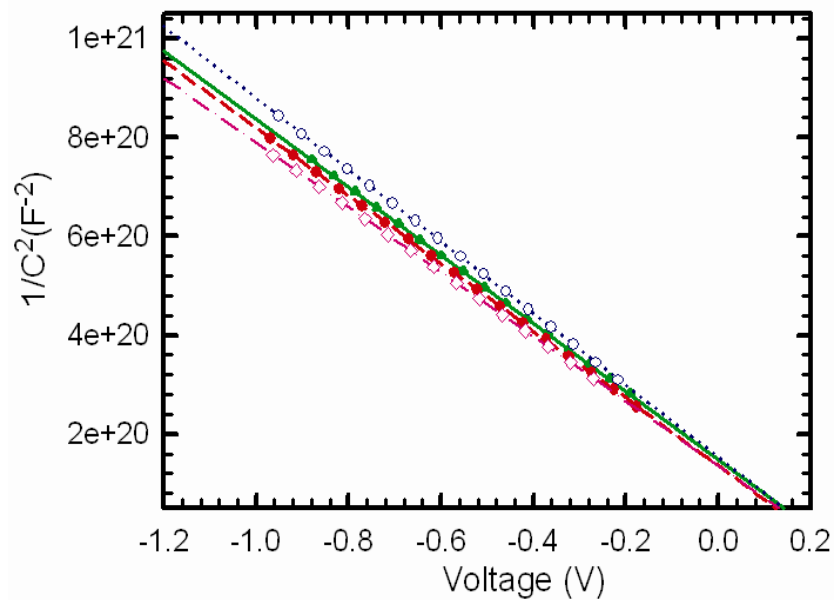

Fig. 6.5 *Reverse bias* $C^{-2}-V$ *characteristics for four Ni/n-Ge (100) Schottky diodes recorded at a frequency of 1 MHz and room temperature.*

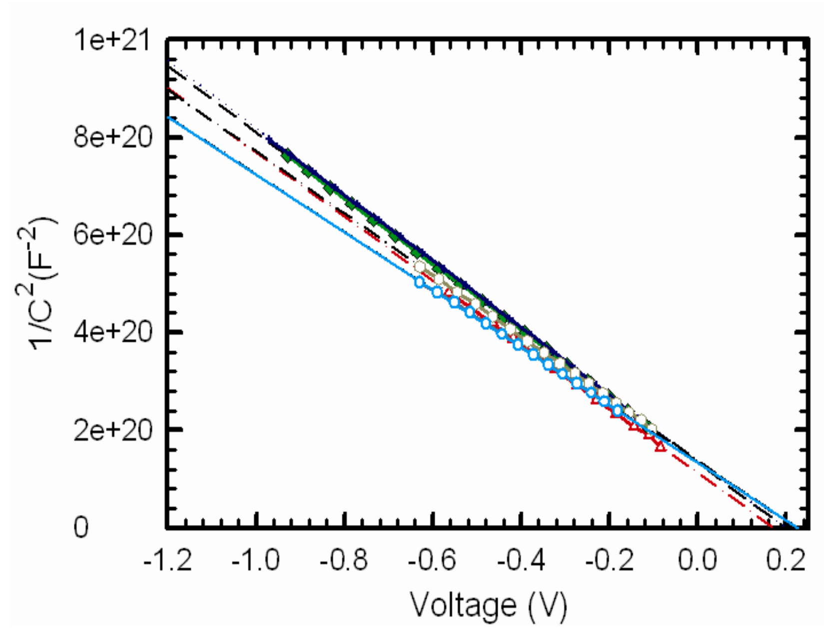

Fig. 6.6 *Reverse bias* $C^{-2}-V$ *characteristics for samples Au/n-Ge (100) Schottky diodes recorded at a frequency of 1 MHz and room temperature.*

The probability of SBH $P(\Phi_B)$ has the form [31,32]:

$$P(\Phi_B) = \frac{1}{\sigma\sqrt{2\pi}} \exp\left\{-\frac{(\Phi_B - \overline{\Phi}_B)^2}{2\sigma^2}\right\}, \tag{6.10}$$

where $\overline{\Phi}_B$ is the mean value of SBH, σ is the standard deviation and $1/\sigma\sqrt{2\pi}$ is the normalization constant. The statistical analysis of the *I-V* BHs for Pd/n-Ge (100), Ni/n-Ge (100) and Au/n-Ge (100) reveals the mean SBH values of 0.541 ± 0.012 eV, 0.503 ± 0.006 eV and

0.549 ± 0.030 eV, respectively.

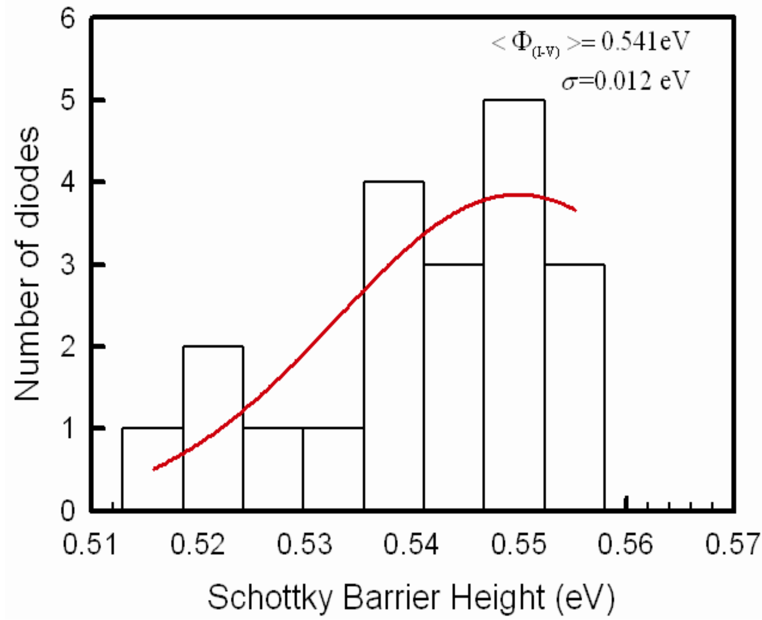

Fig. 6.7 *Distribution of barrier heights from the forward bias I-V characteristics of the Pd/n-Ge (100) Schottky barrier at room temperature.*

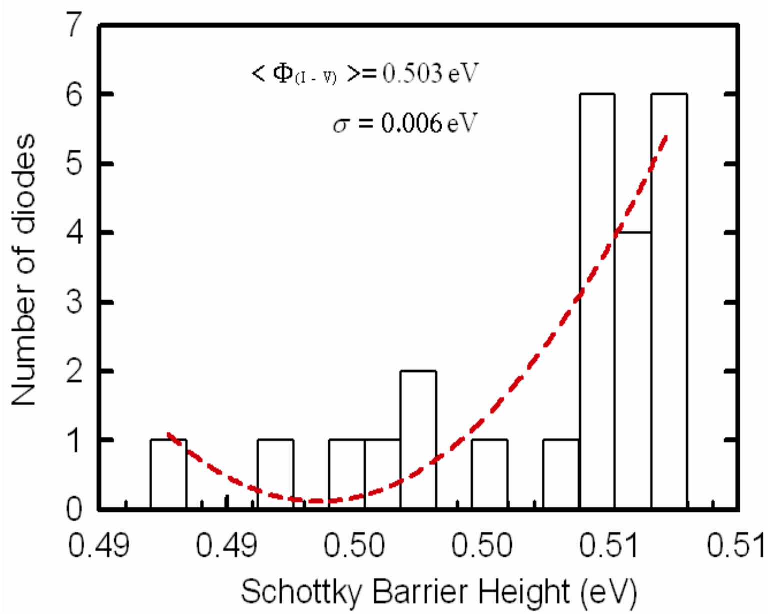

Fig. 6.8 *Distribution of barrier heights from the forward bias I-V characteristics of the Ni/n-Ge (100) Schottky barrier at room temperature.*

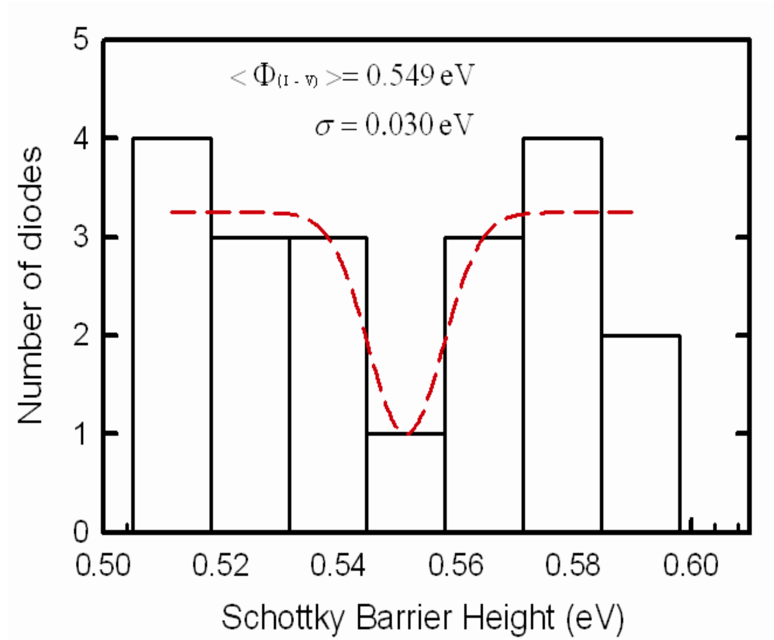

Fig. 6.9 *Distribution of barrier heights from the forward bias I-V characteristics of the Au/n-Ge (100) Schottky barrier at room temperature.*

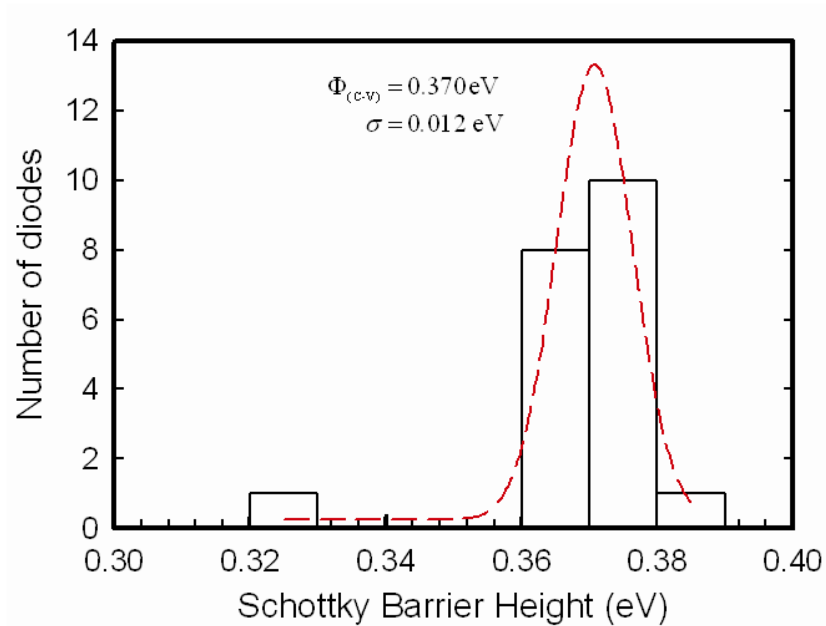

Fig. 6.10 *Distribution of barrier heights from the reverse bias* $C^{-2}-V$ *characteristics of the Pd/n-Ge (100) Schottky barrier recorded at 1 MHz and room temperature.*

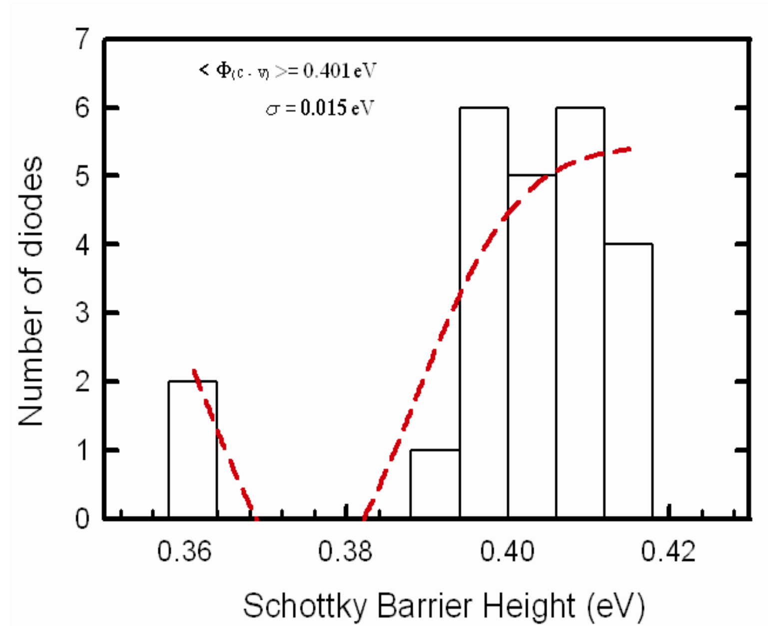

Fig. 6.11 *Distribution of barrier heights from the reverse bias* $C^{-2}-V$ *characteristics of the Ni/n-Ge (100) Schottky barrier recorded at 1 MHz and room temperature.*

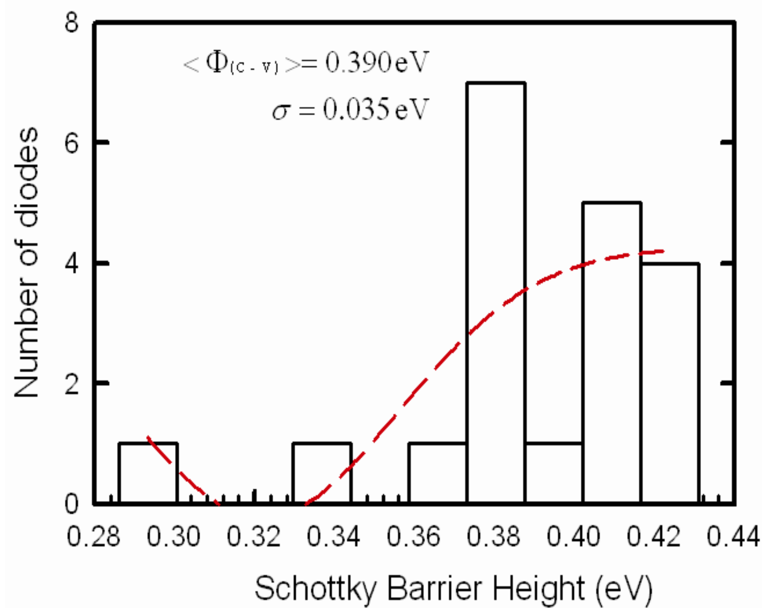

Fig. 6.12 *Distribution of barrier heights from the reverse bias* $C^{-2}-V$ *characteristics of the Au/n-Ge (100) Schottky barrier recorded at 1 MHz and room temperature.*

In the distribution of the BHs from the reverse bias $C^{-2} - V$ characteristics at 1 MHz (Figs. 6.10 - 6.12), the statistical analysis of BHs for Pd/n-Ge (100), Ni/n-Ge (100) and Au/n-Ge (100) yielded mean BH values of 0.370 ± 0.012 eV, 0.401 ± 0.015 eV and 0.390 ± 0.035 eV, respectively. Due to the different nature of the measurement techniques (*I-V* and *C-V*), BHs deduced from them are not always the same [18]. Although, in general BHs from *C-V* measurements are higher than BHs from *I-V* measurements, in this study we obtained *I-V* BHs which are higher than the BHs from *C-V* measurements. Therefore, further studies are needed to clarify these results.

Figs. 6.13 - 6.15 show the statistical distribution of ideality factors from the forward bias *I-V* characteristics for Pd/n-Ge (100), Ni/n-Ge (100) and Au/n-Ge (100), respectively. Gaussian distribution was used to obtain a fit to the histograms. The statistical analysis of the ideality factors for Pd/n-Ge (100), Ni/n-Ge (100) and Au/n-Ge (100) yielded average values of 1.239 ± 0.146, 1.422 ± 0.064 and 1.535 ± 0.263, respectively.

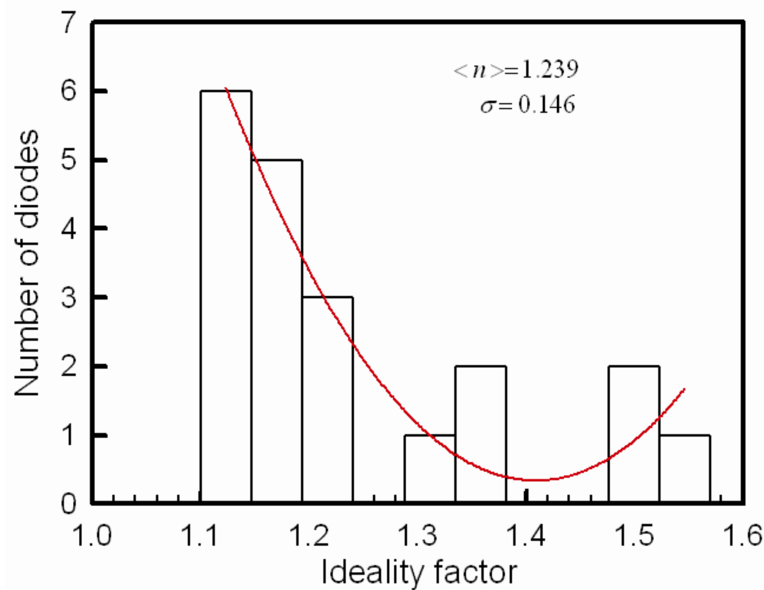

Fig. 6.13 *Distribution of ideality factors from the forward bias I-V characteristics of the Pd/n-Ge (100) Schottky barrier diodes at room temperature.*

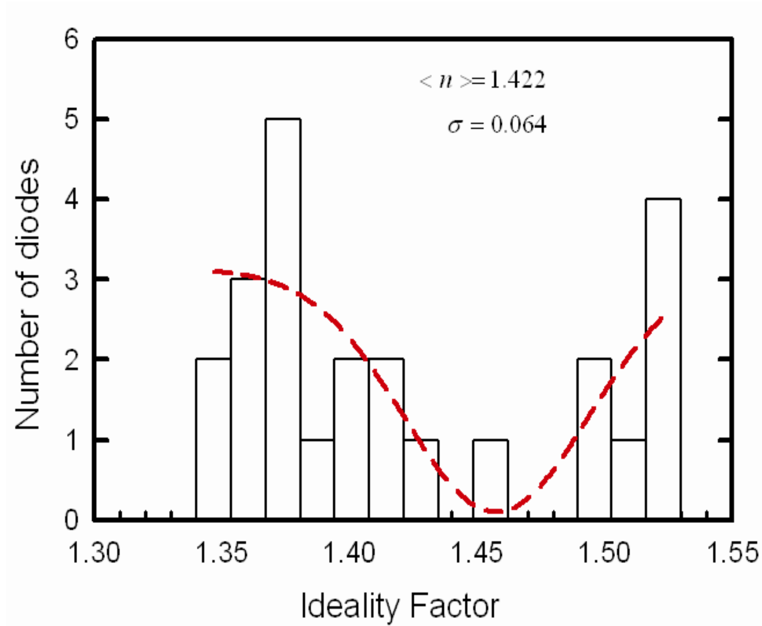

Fig. 6.14 *Distribution of ideality factors from the forward bias I-V characteristics of the Ni/n-Ge (100) Schottky barrier at room temperature.*

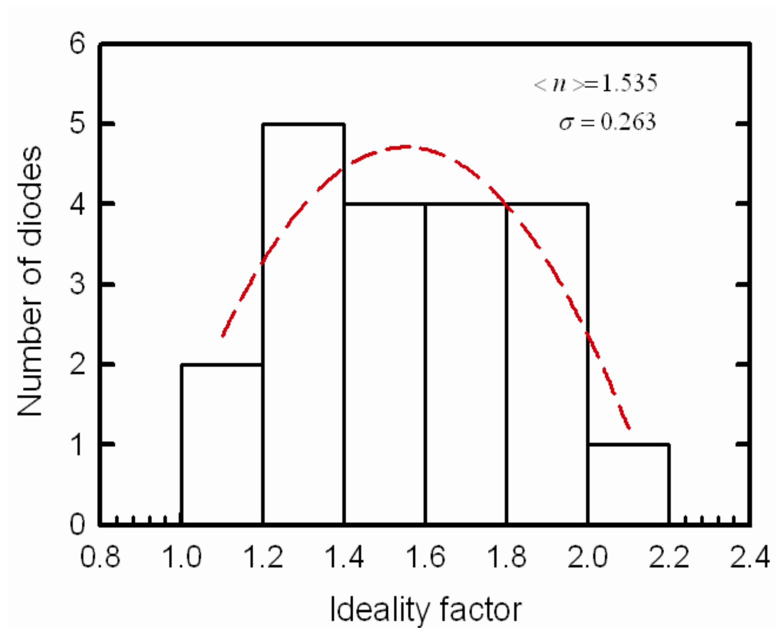

Fig. 6.15 *Distribution of ideality factors from the forward bias I-V characteristics of the Au/n-Ge (100) Schottky barrier at room temperature.*

The data clearly show that the diodes have ideality factors that are considerably larger than 1.01, the value determined by the image effect alone [1,2,11, 17,29,32]. The ideality factor determined by image-force effect should be close to 1.01 or 1.02 [21]. Therefore these diodes are patchy [21,14,15,25]. Schottky contacts, ideality factor greater than 1.0 indicate that the transport properties are not well modelled by thermionic emission alone although the contacts remain rectifying [33]. Explanations for the deviations of the ideality factor from unity ranged from assumptions of a generation-recombination current in the space-charge region [17,29,34], interface dielectric layers or field emission [17] or thermionic field emission [35] due to secondary mechanisms at the interface [5,15]. For example, interface defects may lead to a lateral inhomogeneous distribution of SBHs at the interface resulting in excess current leading to a deviation from ideal thermionic emission behaviour at low voltages and temperatures.

Figs. 6.16 - 6.18 show plots of the *I-V* effective barrier heights as a function of the respective ideality factors for Pd/n-Ge (100), Ni/n-Ge (100) and Au/n-Ge (100), respectively. The straight lines are least-squares fit to the experimental data. The SBHs decreases as the ideality factors increase. That is, there is a linear relationship between experimental effective SBHs and ideality factors of Schottky contacts [26].

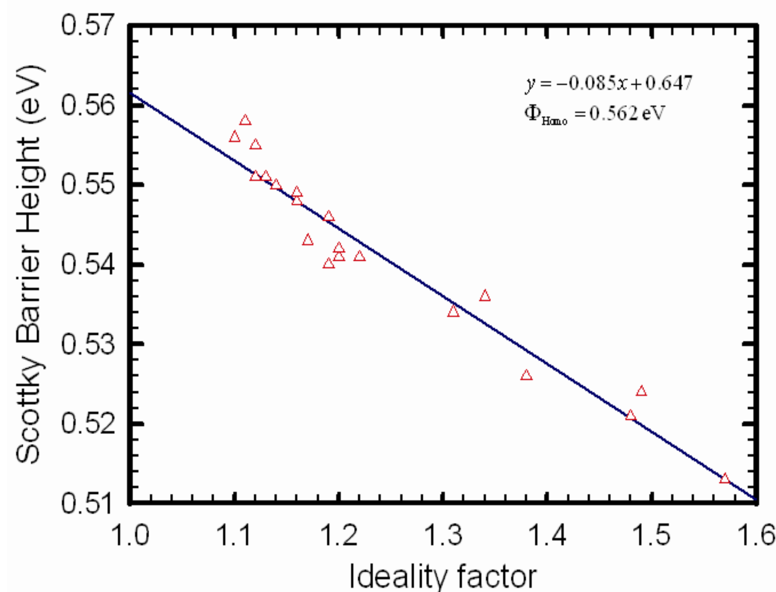

Fig. 6.16 *The experimental I-V Schottky barrier heights versus the ideality factors plot of the Pd/n-Ge (100) Schottky diodes for the barrier inhomogeneity model.*

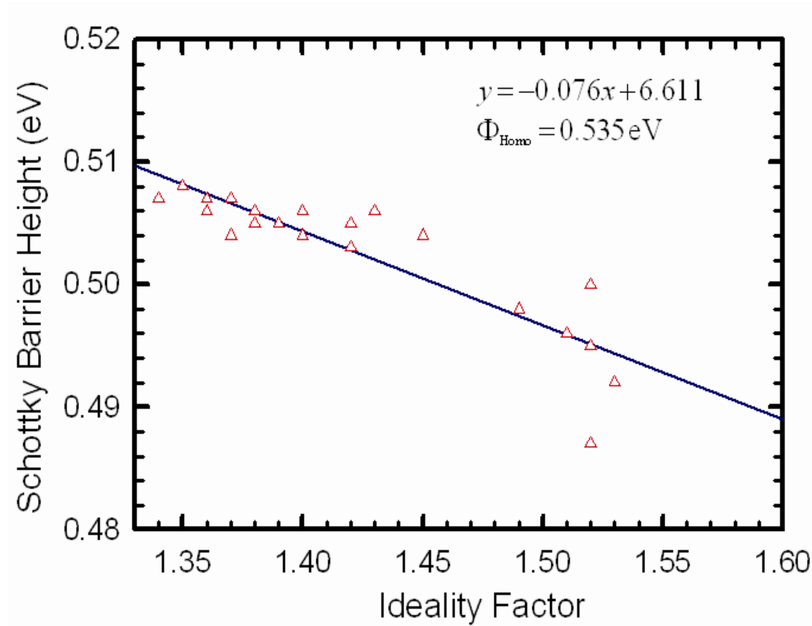

Fig. 6.17 *The experimental Schottky barrier heights versus the ideality factors plot of the Ni /n-Ge (100) Schottky diodes for the barrier inhomogeneity model*

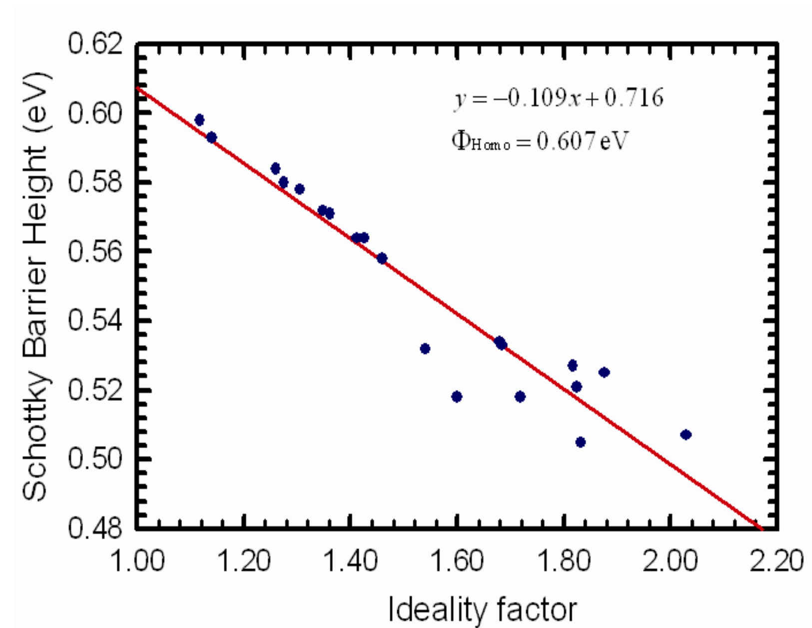

Fig. 6.18 *The experimental Schottky barrier heights versus the ideality factors plot of the Au /n-Ge (100) Schottky diodes for the barrier inhomogeneity model.*

Güler et al. [18] also mentioned that higher ideality factors among identically prepared diodes were often found to accompany lower observed SBHs. This may be attributed to lateral inhomogeneities of the effective SBHs in Schottky barrier diodes [1,12,13,15,36]. Such behaviours of SBH and ideality factors can be explained by means of bias dependence of saddle-point of an inhomogeneous SBH [1,12]. Mönch et al [21] have also proposed that interface defects induced during contacts fabrication could exist in addition to metal-induced gap states (MIGS) and alter the SBH. The defects give rise to additional discrete levels in the band gap and the Fermi level is pinned to one of these levels, possibly quite far away from the charge neutrality level [16]. Laterally homogeneous BH values of 0.562 eV, 0.535 eV and 0.607 eV for Pd/n-Ge (100), Ni/n-Ge (100) and Au/n-Ge (100) Schottky structures, respectively, were obtained from the extrapolation of the plots (Figs. 6.16 - 6.18) to n = 1.00. The homogeneous barrier heights, rather than effective SBHs, of individual contacts or mean values should be used to discuss theories on the physical mechanisms that determine the SBHs of MS contacts [25,27].

6.3 Summary and conclusions

Pd, Ni and Au Schottky diodes on n-Ge (100) were fabricated by resistive deposition under experimentally identical conditions. The BHs and ideality factors values were obtained from individual *I-V* characteristics of MS contacts. It has been shown that BHs and ideality factors varied from diode to diode even though they are were identically fabricated. Laterally homogeneous SBH values of 0.562 eV, 0.535 eV and 0.607 eV were obtained for Pd/n-Ge (100), Ni/n-Ge (100) and Au/n-Ge (100) Schottky structures, respectively, from the linear relationship between the *I-V* effective BHs and ideality factors, which can be explained by lateral inhomogeneities.

The statistical analysis of the *I-V* BHs for Pd/n-Ge (100), Ni/n-Ge (100) and Au/n-Ge (100) yielded mean SBH values of 0.541 ± 0.012 eV, 0.503 ± 0.006 eV and 0.549 ± 0.030 eV, respectively. Ideality factors for Pd/n-Ge (100), Ni/n-Ge (100) and Au/n-Ge (100) Schottky contacts yielded average values of 1.239 ± 0.146, 1.422 ± 0.064 and 1.535 ± 0.263, respectively. In the distribution of the BHs from the reverse bias $C^{-2} - V$ characteristics at 1 MHz, the statistical analysis of BHs for Pd/n-Ge (100), Ni/n-Ge (100) and Au/n-Ge (100) yielded mean SBH values of 0.370 ± 0.012 eV, 0.401 ± 0.015 eV and 0.390 ± 0.035 eV, respectively.

Furthermore, it has been shown experimentally that the data on Pd/n-Ge (100), Ni/n-Ge (100) and Au/n-Ge (100) contacts become an interesting experimental illustration of the theoretical predictions.

References

[1] R.T. Tung, Mater. Sci. Eng. R **35** (2001) 1.

[2] E.H. Rhoderick, R.H. Williams, Metal-Semiconductor Contacts, Claredon Press, Oxford, 1988.

[3] G.A. Baraff, M. Schlüter, Phys. Rev. B. **33** (1986) 7346.

[4] R.L. Van Meirhaeghe, W.H. laflere, F. Cardon, J. Appl. Phys. **76** (1994) 403

[5] S. Chand, S. Bala, Physica B **390** (2007) 179.

[6] J.M. Werner, H.H. Guttler, J. Appl. Phys. **69** (1991) 1522.

[7] J.M. Werner, H.H. Guttler, J. Appl. Phys. **69** (1991) 1522.

[8] S. Chand, J. Kumar, J. Appl. Phys. **82** (1997) 2005.

[9] H. Çetin, E. Ayyildiz, Semicond. Sci. Technol. **20** (2005) 625.

[10] R.T. Tung, Phys. Rev. B. **45** (1992) 13509.

[11] Y.P. Song, R.L. Van Meirhaeghe, W.H. Laflere, F. Cardon, Solid-State Electron **29** (1986) 633.

[12] J.P. Sullivan, R.T. Tung, M.R. Pinto, W.R. Graham, J. Appl. Phys. **70** (1991) 7403.

[13] T.U. Kampen, W. Mönch, Surf. Sci. **333** (1995) 490.

[14] W. Mönch, Phys. Rev. B **37** (1988) 7129.

[15] W. Mönch, J. Vac. Sci. Technol. B **17** (1999) 1867.

[16] M. Sa lam, F.E. Cimili, A. Türüt, Physica B **348** (2004) 397.

[17] B. Boyarbay, H. Cetin, M. Kaya, E. Ayyildiz, Microelectron. Eng. **85** (2008) 721.

[18] G. Güler, Ş. Karataş, Ö. Güllül, Ö. F. Bakkaloğlu, J. All.Com. doi:10.1016/j.jallcom.2009.06163

[19] Ş. Altindal, H. Kanbur, A. Tataroğlu, M.M. Bülbül, Physica B **399** (2007) 146.

[20] A. Tataroğlu, Ş. Altindal, J. Alloys Compd. **479** (2009) 893.

[21] W. Mönch, Semiconductor Surf. And Interfaces, 2nd ed. Springer, Berlin 1995.

[22] T.U. Kampen, W. Mönch, Surf. Sci. **331-333** (1995) 490.

[23] K. Akkilic, M.E. Aydin, A. Turut, Physica Scripta. **70** (2004) 364.

[24] W.P. Leroy, K. Opsomer, S. Forment, R.L. Van Meirhaeghe, Solid-State Electron. **49** (2005) 878.

[25] R.F. Schmitsdorf, T.U. Kampen, W. Mönch, **15** (1997) 1221.

[26] S. Asubay, Ö. Güllü, A. Turut, Appl. Surf. Sci. **254** (2008) 3558.

[27] H. Çetin, B. Şahin, E. Ayyildiz, A. Türüt, Semicon. Sci. Technol. **19** (2004) 1113.

[28] Germanium Silicon: Physics and Materials, Semiconductors and Semi-metals Vol. 56, edited by R. Hull and J.C. Bean (Academic, San Diego, 1999)

[29] S.M. Sze, Physics of Semiconductor Devices, 2nd ed. Wiley, New York, 1981.

[30] V. Saxena, R. Prakash, Polym. Bull. **45** (2000) 267.

[31] H.H. Güttler, J.H. Werner, Appl. Lett. **56** (1990) 1113.

[32] J.H. Werner, H.H. Güttler, J. Appl. Phys. **69** (1991) 1522.

[33] H. Doğan, N. Yildirim, A. Türüt, Microelectron. Eng. **85** (2008) 655.

[34] E. Hökelek, G.Y. Robinson, Solid-State Electron. **99** (1981) 24

[35] E. Ayyildiz, H. Çetin, Zs. Horváth, J. Appl. Surf. Sci. **252** (2005) 1153.

[36] G. Güler, Ö. Güllü, Ö.F. Bakkaloglu, A. Türüt, Semicon. Sci. Technol. **19** (2008) 1113.

List of publications

1. **A. Chawanda**, J.M. Nel, F.D. Auret, W. Mtangi, C. Nyamhere, M. Diale and L. Leach, Journal of the Korean Physical Society 57 **61** (2010) 1970.

CHAPTER 7: RESULTS

Studies of defects induced in Sb doped Ge during contacts fabrication and annealing process.

7.1 Introduction

The high carrier mobility at low electric field [1], and the low effective mass of holes in Ge has opened up possibility of using Ge in ultrafast complimentary metal-oxide-semiconductor (CMOS) devices [2]. This has led to renewed interest in the complete understanding of dynamic properties of radiation and process-induced defects in Ge because defects ultimately determine the performance of devices. Depending on the application, these defects may either be beneficial or detrimental to optimum device functioning [3]. For example, for Si it has been shown that the defects introduced during high-energy electron and proton irradiation increases the switching speed of devices [4]. A lot of research work has been performed on the electrical properties of defects introduced during high-energy, electron and proton irradiation of Ge [5,6,7,8,9,10]. The defects introduced during electron beam deposition of Pt Schottky contacts on n-Ge and the electronic properties of defects introduced during the implantation of Ge with heavier ions, such as dopants have also been reported [3,11]. Metallization is a critical processing step in semiconductor industry. Electron beam deposition (EBD), Sputter deposition and Resistive evaporation are commonly used metallization methods. EBD and Sputter deposition methods introduce defects in semiconductors. Defects introduced in Ge during metallization processes have been investigated [12,13,14,15,16,17]. In this study we investigate on the defects introduced in Ge during contacts fabrication and annealing process, since a practical concern is whether the germanidation process introduces defects, because this may affect the leakage current of the source-drain junctions.

7.2 Experimental procedures

We have used bulk grown n-type Ge with (100) crystal orientation, doped with antimony, (Sb) to a density of 2.5×10^{15} cm^{-3} supplied by Umicore. Before metallization the samples were first degreased and then etched in a mixture of H_2O_2(30%):H_2O (1:5) for 1 minute. Immediately after cleaning they were inserted into a vacuum chamber where AuSb (0.6% Sb), 100 nm thick was deposited by resistive evaporation as back ohmic contacts. The samples were then annealed at 350°C in Ar ambient for ten minutes to minimize the ohmic contact resistivity [3]. Before Schottky contacts deposition, the samples were again chemically cleaned as described above. Cobalt (Co) and ruthenium (Ru) Schottky contacts were deposited onto the Ge in an electron beam deposition system, while palladium (Pd) and some Co Schottky contacts were deposited by vacuum resistive evaporation. These contacts were deposited under vacuum at a pressure below 10^{-6} Torr. The contacts were 0.6 mm in diameter and 30 nm thick. Following contact fabrication, current-voltage (*I-V*) and capacitance-voltage (*C-V*) measurements were performed to assess the quality of the diodes and to determine the free carrier density of the Ge, respectively. Thereafter, electrical characterization was repeated after every isochronal annealing cycle in Ar ambient for 30 minutes between room temperature and 600°C. Both conventional deep-level transient spectroscopy (DLTS) [18] and Laplace-DLTS (LDLTS) [19,20] were used to study the defects introduced in the Ge during the contact fabrication and annealing process. The '*signatures*' of metallization induced defects (i.e. energy position in band gap relative to the conduction band and valence band for the electron and hole traps, respectively, E_T, and their apparent capture cross section, σ_a) were determined from the Arrhenius plots of $\ln(T^2/e)$ *versus* $1000/T$, where '*e*' is either the hole or electron emission rate, and T is the measurement temperature in K.

7.3 Results and discussions

In this section the electronic and annealing properties of defects introduced in n-type Ge during electron beam deposition and annealing process are presented. In the nomenclature used here "*E*" means electron trap and the number following it is the energy level of this trap below the conduction band. Similarly, "*H*" means hole trap and number following it is the energy level of this trap above the valence band.

7.3.1 Pd/n-Ge (100) Schottky diodes

Fig. 7.1 shows a conventional DLTS spectrum obtained from Pd Schottky contacts annealed from room temperature to 350°C. Fig. 7.1 (a) depicts that no defects are observable (within the detection limit of our DLTS system which is approximately >10^{11}cm^{-3}) for resistively evaporated Pd Schottky contacts, indicating that the Ge is of high quality [12]. A hole trap *H*(0.33) with capture cross-section of 1.0 × 10^{-14} cm^{-2} was observed after annealing at 300°C. Although Churms et al. [21] reported Pd-Ge inter-diffusion at 300°C anneal during a study of Pd/Ge interaction by microbeam Rutherford backscattering spectrometry, we propose to assign this hole trap to vacancy (V)- related defect complex, since it annealed out after a 350°C anneal. Also, it has been suggested by [1] that the germanide formation causes the injection of vacancies into the semiconductor bulk and, hence the occurrence of V-related defects. The annealing studies were carried out up to 525°C to determine if there are any other defects induced in Ge during the annealing process.

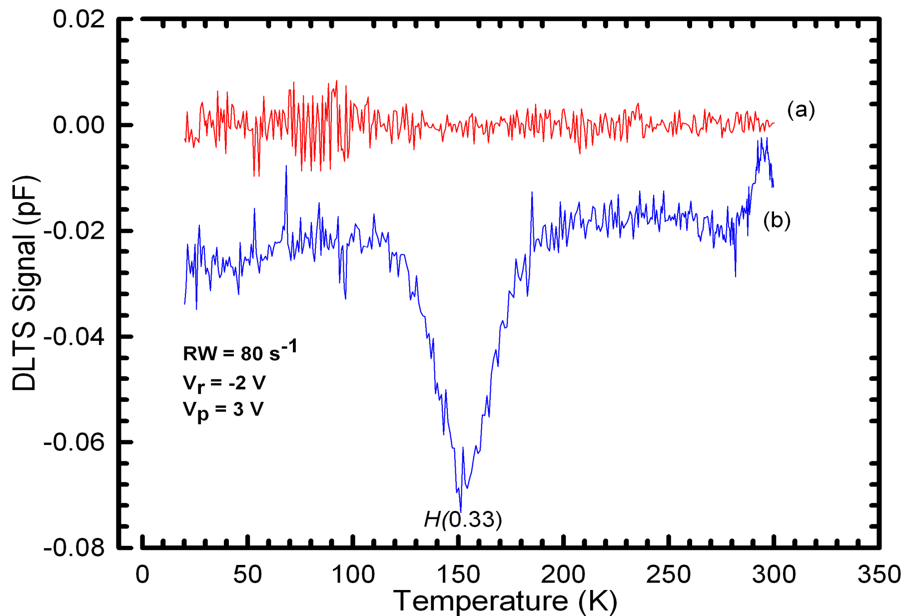

Fig. 7.1 *DLTS spectra of the Pd Schottky contacts on n-Ge (100) (a) as-deposited and (b) after annealing at 300°C. These spectra were recorded at a rate window of 80s^{-1} and quiescent reverse bias of –2 V with a filling pulse of 3 V.*

7.3.2 Co/n-Ge (100) Schottky diodes

An electron trap at *E*(0.37) and a hole trap at *H*(0.29) with capture cross sections of 4.0×10^{-14} cm^{-2} and 3.0×10^{-14} cm^{-2}, respectively were observed in as-deposited Co Schottky contacts fabricated with electron beam deposition (EBD), as shown in Fig. 7.2. The defects electronic properties were extracted from the Arrhenius plot shown in Fig. 7.3. The electron trap *E*(0.37) is the well known (=/–) charge state of the *E*-centre (V-Sb) in Sb-doped Ge [15], whilst the hole trap *H*(0.29) corresponds closely to that reported for the H(0.307), the (–/0), the single acceptor level of Sb-V centre in Ge [5,6], created during electron irradition. In the case of electron beam deposition, the *E*-centre forms when energetic particles (originating in the region of the filament) impinge on the Ge, creating vacancies and interstitials at and close to Ge surface [12,22]. These vacancies are mobile at room temperature and migrate into Ge where they combine with Sb-dopant atoms to form Sb-V pairs (*E*-centre) [12,23]. The hole trap *H*(0.29) is thermally stable up to an annealing temperature of 150°C and anneals out at 200°C [24].

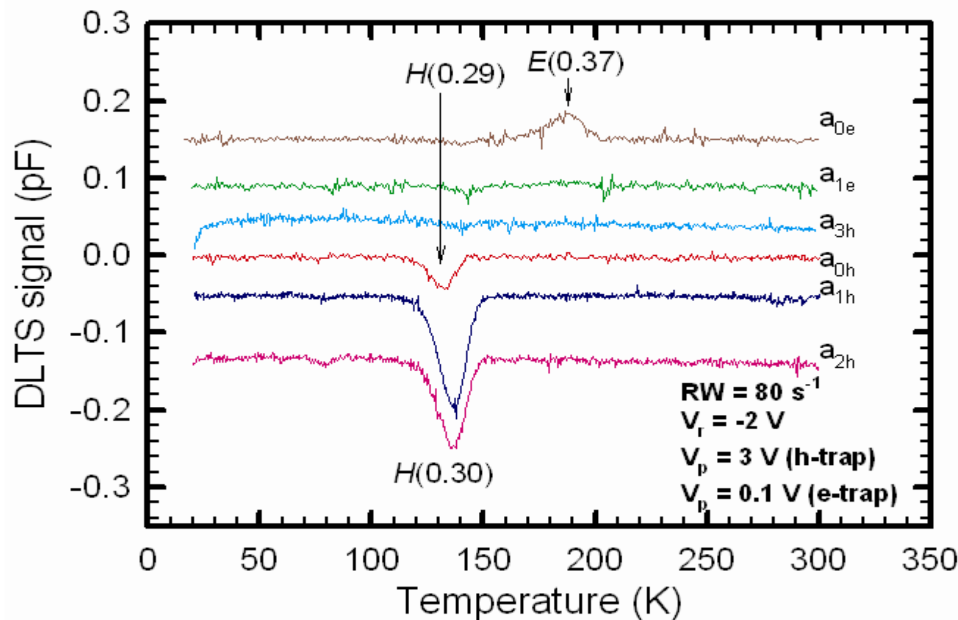

Fig. 7.2 *DLTS spectra of the EBD deposited Co Schottky contacts on n-Ge (100) (a_0) as-deposited and after annealing at (a_1) 200°C, (a_2) 300°C and (a_3) 350°C. The subscripts 'e' and 'h' on the graph labels stand for electron and hole traps, respectively. These spectra were recorded at a rate window of 80 s^{-1} and quiescent reverse bias of –2 V with filling of 0.1 V and 3 V for electron and hole traps, respectively*

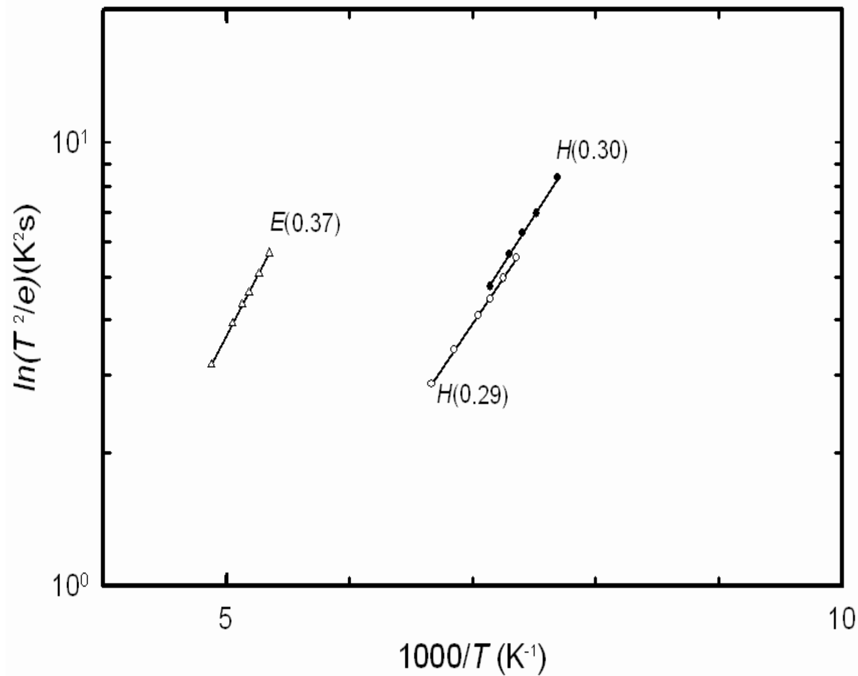

Fig. 7.3 *Arrhenius plot of an electron and hole traps introduced in n-Ge (100) after Co Schottky contact fabrication using EBD and during annealing process.*

Further annealing studies in the temperature range from 200 to 350°C, reveal a hole trap *H*(0.30), shown in Fig. 7.2 with capture cross section of 7.8 × 10^{-14} cm^{-2} which anneals-out between 300 and 350°C.

The signature of the *H*(0.30) defect corresponds to that reported during DLTS studies of cobalt Schottky contacts sputter deposited onto the n-type Ge, after subjecting the contacts to rapid thermal annealing for 30 s at 750°C. This defect is assigned to substitutional Co (Co_s) double acceptor level ($Co_s^{-/2-}$) with activation energy 0.3 eV [25]. Although Opsomer et al. [25] reported Co-Ge in-diffusion of Co sputter deposited on n-type Ge after rapid thermal annealing of the contacts at temperatures higher than 600°C for 30 s, in this study Co-Ge inter-diffusion is revealed after isochronal annealing at a temperature of 350°C for 30 minutes, as shown in RBS studies (see Fig 7.4). This is also in agreement with what was reported by Sun et al [26]. Co atoms will diffuse into bulk Ge at a relatively low temperature of ~ 150°C.

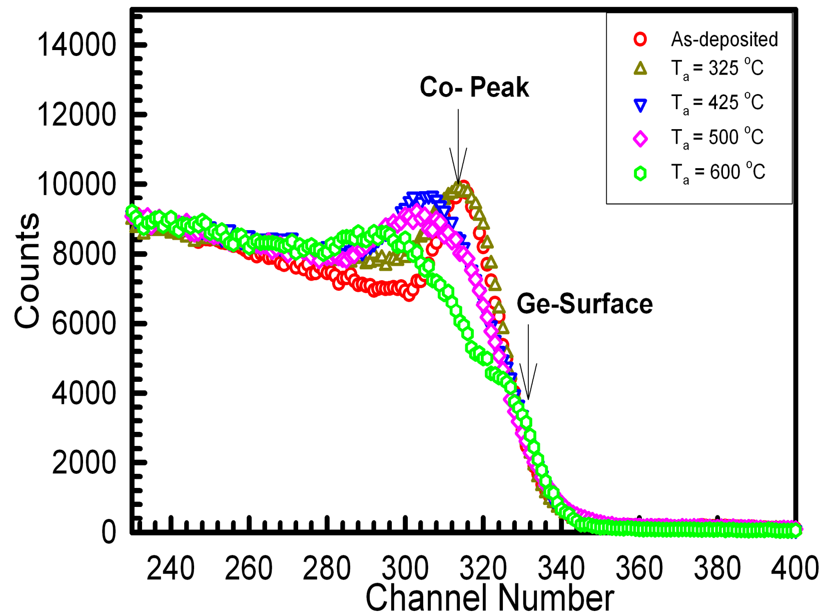

Fig. 7.4 *RBS spectra of 1.6 MeV He$^+$ ions for cobalt films deposited on germanium after isochronal thermal treatment for 30 min at different annealing temperatures: as-deposited, 325, 425, 500, and 600°C.*

Increasing the anneal temperature to 350°C, the hole trap *H*(0.30) completely vanished (Fig. 7.2). The annealing studies were carried out up to 525°C to determine if there are any other defects induced in Ge during the annealing process. After 525°C anneal, the Co Schottky contacts severely deteriorated, and contacts became near ohmic.

7.3.3 Ru/n-Ge (100) Schottky diodes

7.3.3.1 Electron traps

DLTS spectra for electron traps induced in Ge after electron beam deposition of Ru/n-Ge (100) Schottky contacts are depicted in Fig. 7.5. The spectra were recorded for as-deposited, 100, 150, 175, 200, 225, 250, 300 and 350°C. After Ru Schottky contacts fabrication, *E*(0.38) level with capture cross section of 1.0 × 10^{-14} cm^{-2} is the only detectable electron trap. The defect's electronic properties were extracted from the Arrhenius plot shown in Fig. 7.6. This can be attributed to the significant injection of minority carriers into the band gap even without applying a minority carrier filling pulse because of very high barrier height of Ru SBD[27].

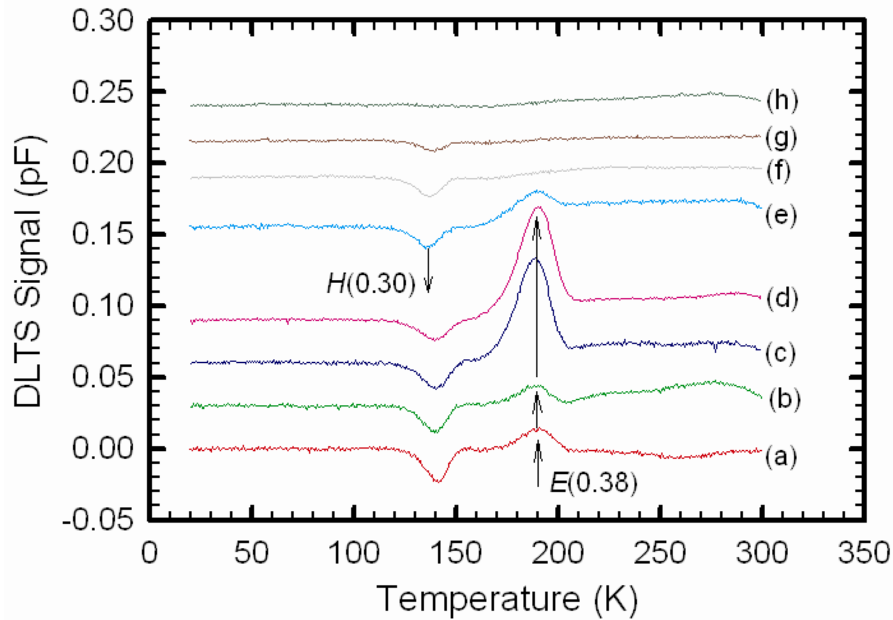

Fig. 7.5 *DLTS spectra for electron traps after electron beam deposition of Ru Schottky contacts on n-Ge (100) (a) for as-deposited, and after annealing at (b) 100°C, (c) 150°C, (d) 175°C, (e) 200°C, (f) 225°C, (g) 250°C, (h) 300°C and (i) 350°C. These spectra were recorded with a quiescent reverse bias of –2 V, at a rate window of 80 s^{-1}, a pulse voltage of –0.15 V and pulse width of 1 ms.*

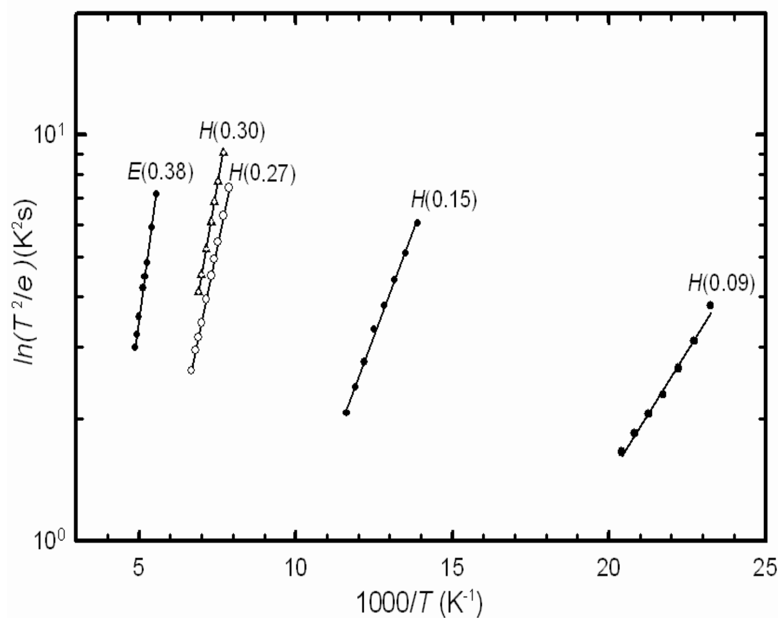

Fig. 7.6 *Arrhenius plot of an electron and hole traps (Fig. 7.5 & Fig. 7.10) introduced in n-Ge (100) after Ru Schottky contacts fabrication using EBD.*

7.3.3.2 Annealing mechanism of the E-centre (E (0.38))

The *E*-centre (*E*(0.38)) is a very important defect in Ge for its role in dopant deactivation and free carrier removal as for each V-Sb complex formation results in the removal of three free carriers [6]. It is therefore important to establish the annealing mechanism of the *E*-centre. The concentration as function of depth profile of the E-centre, measured at different isochronal annealing temperatures is shown in Fig. 7.7. It can be seen that the depth profile for as-deposited samples shows that the defect concentration decreased from the Ge surface, and this proves that the energetic particles emerging from the filament during contact fabrication creates vacancies on and beneath the semiconductor surface [28]. The defect concentration profile (Fig 7.7) shows an increase in defect concentration deeper into the bulk material as the annealing temperature is increased. This is attributed to the diffusion of the *E*- centre into the semiconductor as it become mobile at elevated temperatures. A 175°C anneal, with prolonged annealing time results in a broadened profile which shifted to lower concentration. Therefore, further investigations need to be carried out to establish defect concentration profile annealing mechanisms for prolonged time model.

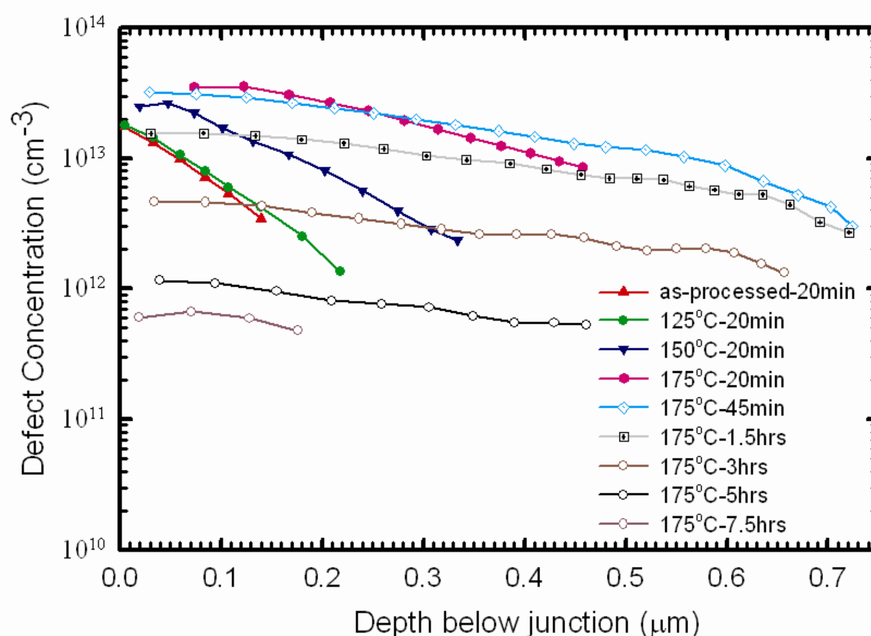

Fig. 7.7 *Depth profile for E(0.38) at different annealing temperatures. The measurements were performed by LDLTS at fixed temperature of 195 K.*

To further understand the annealing mechanism of the *E*-centre it was important to investigate the annealing kinetics of the defect and determine the activation energy for the annealing process. Fig. 7.8 (a) shows the results for the annealing kinetics at temperatures 160°C, 170°C and 175°C, from which the annealing rate (*K*) for each temperature was extracted and used for the construction of the Arrhenius plots shown in Fig 7.8 (b).

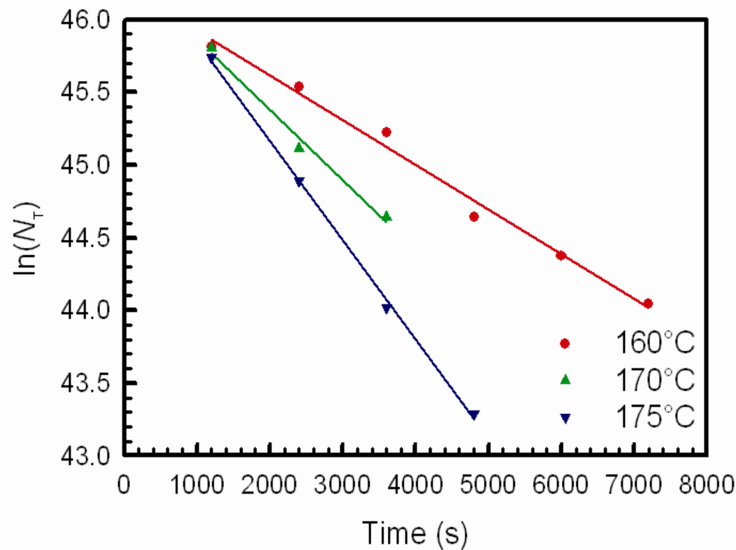

Fig. 7.8 (a) *Semi-log plot of defect concentration profiles against annealing time measured at annealing temperatures of 160°C, 170°C and 175°C from which the annealing rate constant, K is calculated.*

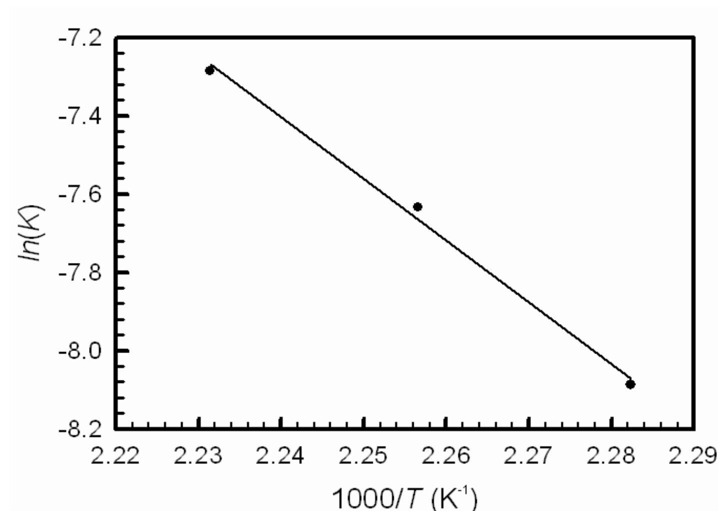

Fig. 7.8 (b) *The Arrhenius plot of ln (K) versus 1000/T*

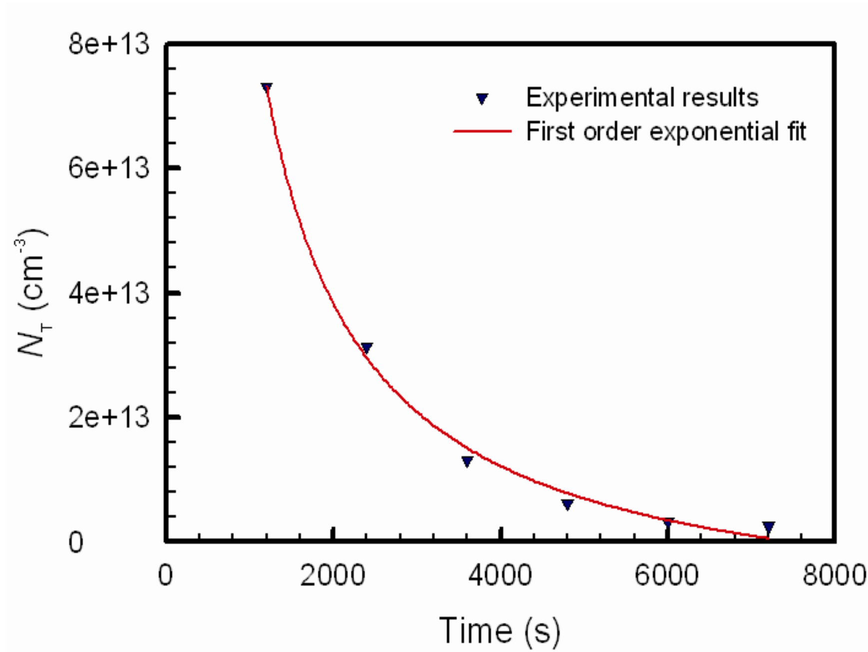

Fig. 7.8 (c) *The plot of defect concentration against annealing time at annealing temperature of 175°C*

The annealing of the *E*-centre follows a first order exponential decay as depicted in Fig 7.8 (c) with activation energy E_a = 1.36 eV and pre-exponential factor $A = (1.2 \pm 0.3) \times 10^{12} s^{-1}$ extracted from the slope and vertical axis intercept of the Arrhenius plot (Fig. 7.8 (b), respectively. The value of the pre-exponential factor *A*, is just below the lower end of the purely dissociation range of > 10^{12} s^{-1} [29].

7.3.3.3 Causes of EBD damage

The following energetic gaseous ions were reported by [30] to be in the chamber during the EBD process: H, H_2, C, N, O, OH, H_2O, CO, N_2, CO_2 and C_xH_y. H and H_2 are the positive ions, and negative ions are: O, OH, C and C_xH_y. Due to these energetic gaseous ions, which also reach the substrate during the EBD, vacancies are created on and beneath the semiconductor surface.

Fig. 7.9 (a & b) shows the TRIM (Transport of Ion in Matter) (version 2006.02) [31] simulation profiles for regions where vacancies are created in germanium by some residual vacuum gas ions (assuming a maximum energy of 10 keV for ions in the deposition chamber). The projected ion

range is ≈25 nm for carbon, nitrogen and oxygen ions from energy of 10 keV, each ion producing approximately 4 vacancies/nm. Hydrogen ions will create primary damage of up to a depth of ≈ 100 nm. The vacancies and interstitials created will diffuse and form stable defect complexes (e.g. *E*-centre) even deeper than the projected ion range.

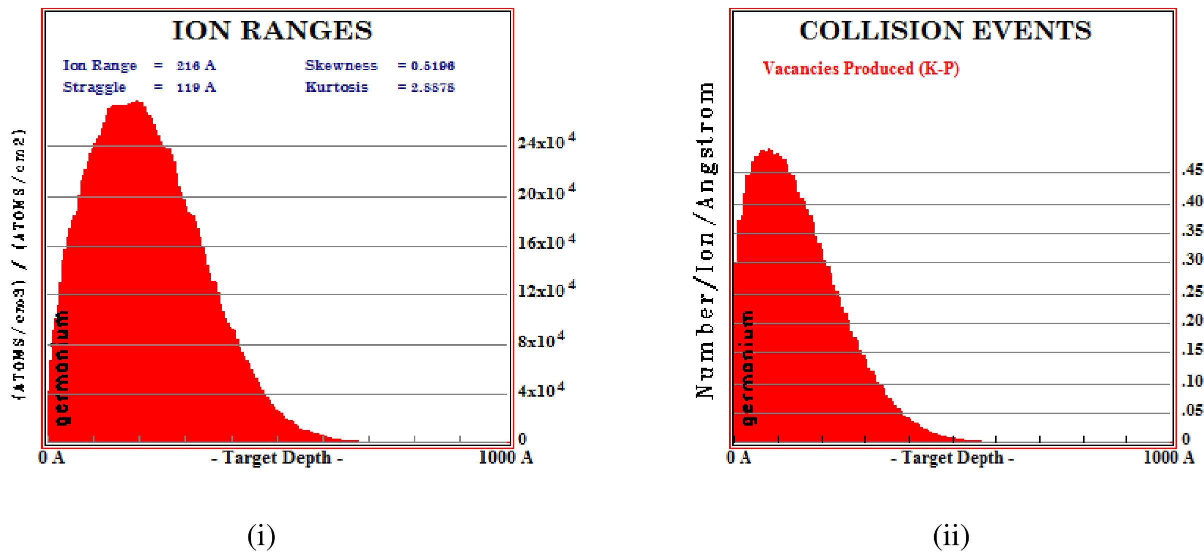

Fig. 7.9 (a) *(i) TRIM simulation for the projected ion range and (ii) damage events of 10 keV oxygen ions in Ge.*

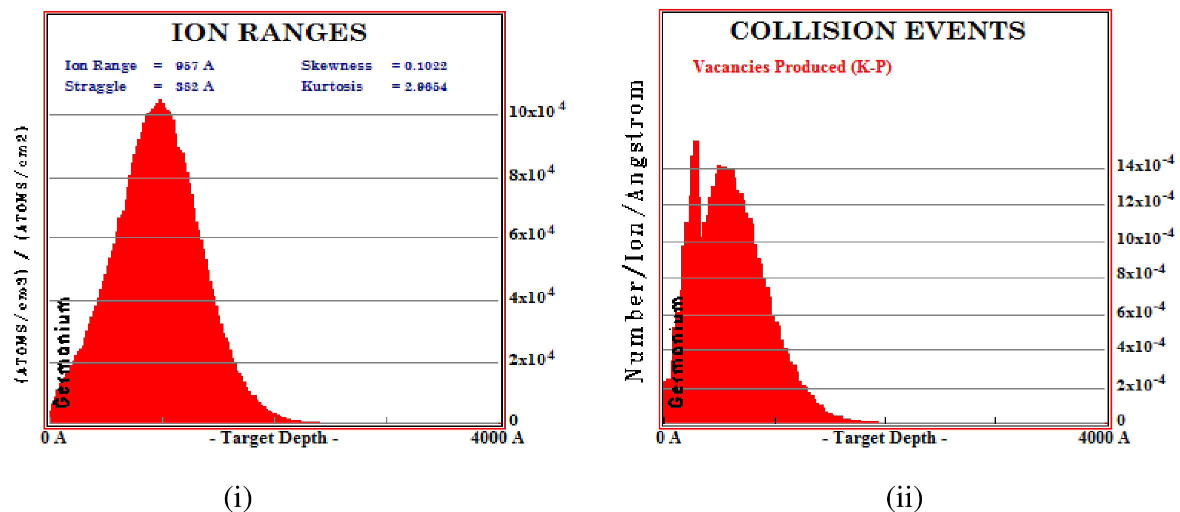

Fig. 7.9 (b) *(i) TRIM simulation for the projected ion range and (ii) damage events of 10 keV hydrogen ions in Ge*

7.3.3.1 Hole traps

Fig. 7.10 and Fig. 7.11 show conventional DLTS and Laplace DLTS spectra, respectively for hole traps introduced in Ge during Ru Schottky contacts EBD deposition. Hole trap *H*(0.30) with capture cross section 6.2 × 10^{-13} cm^{-2} is the prominent single acceptor level of the *E*-centre. The hole traps *H*(0.09), *H*(0.15) and *H*(0.27) with capture cross sections 7.8 × 10^{-13} cm^{-2}, 7.1 × 10^{-13} cm^{-2} and 2.4 × 10^{-13} cm^{-2}, respectively were also observed in as-deposited Ru Schottky contacts. The electronic properties of these defects were obtained from the Arrhenius plots shown in Fig. 7.6. Auret et al. [23] also reported the trap *H*(0.09) after metallization by EBD process. It has been proposed that this defect is the third charge state of the *E*-centre (+/0) [9].

Although the hole trap *H*(0.27) has been reported to be induced after a 200°C anneal of MeV electron irradiated Ge sample [27], in this study the defect was induced during the Ru Schottky contacts fabrication process. This may be due the fact that during EBD the substrate temperature is higher than the room temperature and thus thermally inducing the defect *H*(0.27). The measurement of the hole trap *H*(0.27) in the presence of *H*(0.30) was achieved by LDLTS which clearly separates the signals

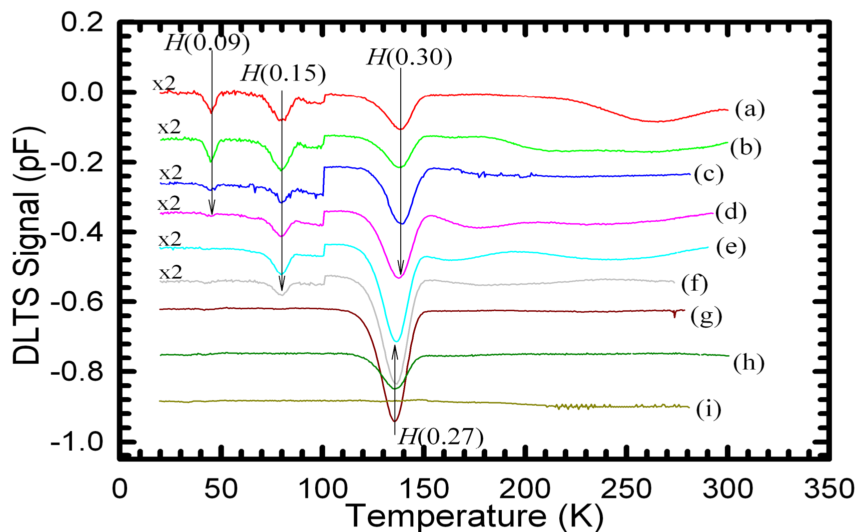

Fig. 7.10 *DLTS spectra for the hole traps induced in n-Ge (100) after electron beam deposition of Ru Schottky contacts. The spectra were recorded (a) for as-deposited, and after annealing at (b) 100°C, (c) 150°C, (d) 175°C, (e) 200°C, (f) 225°C, (g) 250°C, (h) 300°C and (i) 350°C. The spectra were recorded with a quiescent reverse bias of –1 V, at a rate window of 80* s^{-1}*, a pulse voltage of 3 V and pulse width of 1 ms.*

Fig 7.11 shows that the peak concentration (peak height) for *H*(0.30) trap is much higher than that of *H*(0.27), hence much larger concentration of *H*(0.30) in the as-deposited samples. The variation of the defect concentration for the hole traps *H*(0.30) and *H*(0.27), and the electron trap *E*(0.38) as a function of annealing temperature is shown is in Fig. 7.12. The concentration of *H*(0.27) increased with annealing temperature until it reached a maximum after a 225°C anneal, at which point the *E*-centre completely vanishes. This confirms what was reported by Coutinho et al. [32] and Markevich et al. [33] that *H*(0.27) is a product of V-Sb after annealing to form a new V-Sb_2 complex which is electrically active [32,33]. After 350°C annealing temperature, all defects had completely annealed out and the annealing was carried out up to 600°C to determine whether there are any other defect levels that might be reactivated after presumably being transformed into inactive complexes during annealing. There were no other defects observed above 350°C annealing temperature.

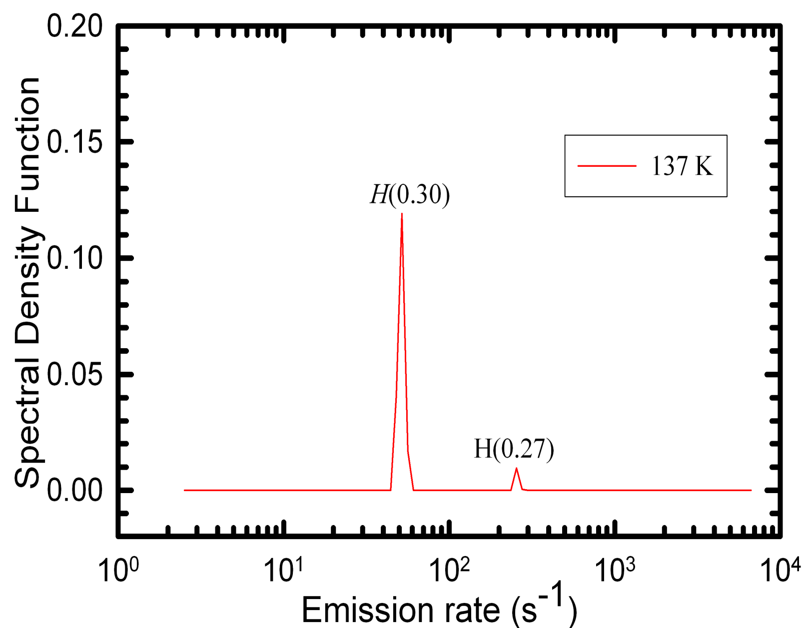

Fig. 7.11 *LDLTS spectra for H(0.27) and H(0.30) in as-deposited sample recorded at 137 K.*

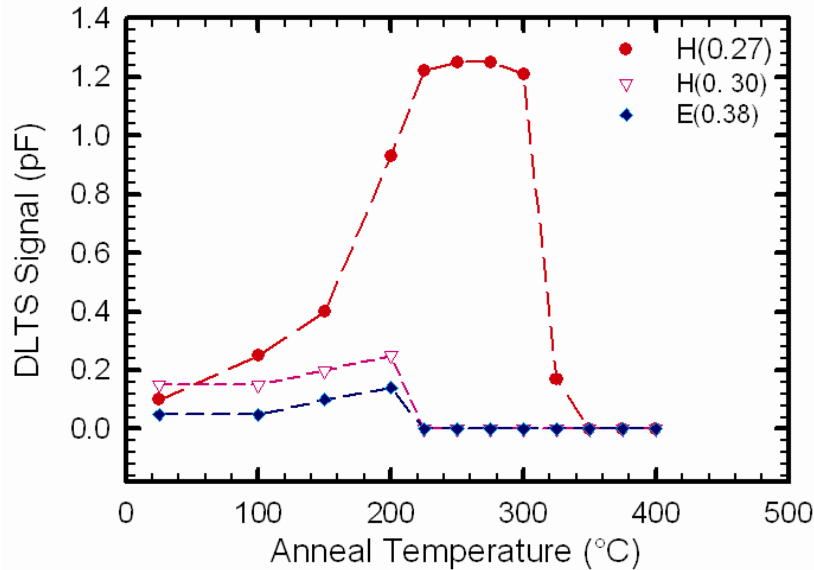

Fig. 7.12 *Variation of defect concentration for H(0.27), H(0.30) and E(0.38) with annealing temperature*

7.4 Summary and conclusions

DLTS and annealing studies of the Pd/n-Ge (100) Schottky contacts reveal the introduction of a hole trap *H*(0.33) at a temperature of 300°C. This hole trap is probably vacancy (*V*)-related defect complex. DLTS analysis on the EBD Co Schottky contacts has shown that an electron trap *E*(0.37) and a hole trap *H*(0.29) were induce in n-Ge during the fabrication of the contacts and a hole trap *H*(0.30) is induced during the annealing process. This defect is assigned to substitutional Co (Co_s) double acceptor level ($Co_s^{-/2-}$) with activation energy 0.3 eV [25].

DLTS and LDLTS revealed that the dominant defect induced by electron beam deposition is the V-Sb (*E*-centre). This depicts that during electron beam deposition vacancies are created below the semiconductor surface by particles which are ionized around the filament and then accelerated by the electric and magnetic fields towards the substrate. A hole trap *H*(0.27), induced during EBD of Ru Schottky contacts shows some reverse annealing between room temperature and 350°C (where it anneals out), reaching a maximum concentration at 225°C. This trap is reported to be due to V-Sb_2 complex. All defects induced in Ru Schottky contacts annealed out after a 350°C anneal.

References

[1] E. Simoen, K. Opsomer, C. Claeys, K. Maex, C. Detavernier, R.L. Van Meirhaeghe, and P. Clauws, J. Electrochem. Soc. **154** (2007) H857.

[2] Germanium silicon: physics and materials. In: Hull R, Bean JC, editors. Semiconductors and semimetals, vol. 56. San Diego: Academic Press; 1999.

[3] F.D. Auret, P.J. Janse van Rensburg, M. Hayes, J.M. Nel, S. Coelho, W.E. Meyer, S. Decoster, V. Matias, A. Vantomme, D. Smeets, Nucl. Instrum. Methds B **257** (2007) 169.

[4] S.J. Pearson, A.J. Tavendale, J. Appl. Phys. **54** (1983) 820.

[5] J. Fage-Pedersen, A. Nylandsted Larsen, A. Mesli, Phys. Rev. B **62** (2000) 10116.

[6] V.P. Markevich, A.R. Peaker, V.V. Litvinov, V.V. Emstev, L.I. Murin, J. Appl. Phys. **95** (2004) 4078.

[7] V.P. Markevich, I.D. Hawkins, A.R. Peaker, K.V. Emstev, V.V. Emstev, V.V. Litvinov, L. Dobaczewski, Phys. Rev. B **70** (2004) 235213-1.

[8] V.P. Markevich, I.D. Hawkins, A.R. Peaker, V.V. Litvinov, L. Dobaczewski, J.L. Lindström, Appl. Phys. Lett. **81** (2002) 1821.

[9] C.E. Lindberg, J. Lundsgaard Hansen, P. Bomholt, A. Mesli, K. Bonde Nielsen, and A. Nylandsted Larsen, Appl. Phys. Lett. **87** (2005) 172103.

[10] F.D. Auret. P.J. Janse van Rensburg, M. Hayes, J.M. Nel, W.E. Meyer, S. Decoster, V. Matias, and A. Vantomme, Appl. Phys. Lett. **89** (2006) 152123.

[11] P. Blood, J.W. Orton, The Electrical Characterization of Semiconductors: Majority Carriers and Electron States, Academic Press, London, 1992.

[12] F.D. Auret, S.M.M. Coelho, P.J. Janse van Rensburg, C. Nyamhere, W.E. Meyer, Mater.

Sci. Semicond. Process. **11** (2008) 348.

[13] F.D. Auret, W.E. Meyer, S.M.M. Coelho, M. Hayes, Appl. Phys. Lett. **88** (2006) 24110.

[14] F.D. Auret, W.E. Meyer, S.M.M. Coelho, M. Hayes, J.M. Nel, Mater. Sci. Semicond. Process, **9** (2006) 576.

[15] F.D. Auret, S.M.M. Coelho, M. Hayes, W.E. Meyer, J.M. Nel, Phys Status Solidi (a), **205** (2008) 159.

[16] F.D. Auret, S. Coelho, W.E. Meyer, C. Nyamhere, M. Hayes, J.M. Nel, J. Electron. Mater. **36** (2007) 1604.

[17] E. Simoen, K. Opsomer, C. Claeys, K. Maex, C. Detavernier, R.L. Meirhaegh et al. Appl. Phys. Lett. **89** (2006) 202114.

[18] D.V. Lang, J. Appl. Phys. **45** (1974) 3023.

[19] L. Dobaczewski, P. Kaczor, I.D. Hawkins, A.R. Peaker, J. Appl. Phys **76** (1994) 194.

[20] L. Dobaczewski, A.R. Peaker, N.K. Bonde, J. Appl. Phys **96** (2004) 4689.

[21] C.L. Churms, C.M. Comrie, R.S. Memutudi, Nucl. Instrum. Methds. B **158** (1999) 713.

[22] C. Christensen, J.W. Petersen, A. L. Nylandsted, Appl. Phy. Lett. **61** (1992) 1426.

[23] F.D. Auret, W.E. Meyer, S. Coelho, and M. Hayes, Appl. Phys. Lett. **88** (2006) 242110.

[24] C. Nyamhere, A. Chawanda, A.G.M. Das, F.D. Auret, M. Hayes, Physica B **401-402** (2007) 227.

[25] K. Opsomer, E. Simoen, C. Claeys, K. Maex, C. Detavernier, R.L. Van Meirhaeghe, S. Forment, P. Clauws, Mater. Sci. Semicond. Process. **9** (2006) 554.

[26] H.P. Sun, Y.B. Chen, X.Q. Pan, D.Z. Chi, R. Nath, Y.L. Foo, Appl. Phys. Lett. **86** (2005) 071904.

[27] C. Nyamhere, PhD Thesis, University of Pretoria, 2009.

[28] C. Nyamhere, A. Chawanda, A.G.M. Das, F.D. Auret, M. Hayes, Physica B **401-402**

(2007) 226.

[29] F.D. Auret and P.N.K. Deenapanray, Crit. Rev in Solid State and Mater. Sci. **29** (2004) 1.

[30] E.M. Sithole, MSc Thesis, University of Pretoria, 2001.

[31] J.P. Biersack and L.G. Haggmark, Nucl. Instrum. Methods. **174** (1980) 257

[32] J. Coutinho, V.J.B. Torres, S. Öberg, A. Carvalho, C. Janke, R. Jones et al. Mater. Sci. Mater. Electron. **18** (2007) 769.

[33] V.P. Markevich, S. Bernardini, I.D. Hawkins, A.R. Peaker, V.I. Kolkovsky, A. Nylandsted Larsen and L. Dobaczewski, Mater. Sci. Semicond. Process. **11** (2008) 354.

List of publications

1. A. Chawanda, C. Nyamhere, F.D. Auret, W. Mtangi, T. Hlatshwayo, M. Diale, J.M. Nel, Physica B **404** (2009) 4482.